RSC Advances

PAPER

View Article Online
View Journal | View Issue

Cite this: *RSC Adv.*, 2016, **6**, 98257

Facile fabrication of robust superhydrophobic surfaces: comparative investigation†

Robin M. Bär,[a] Simon Widmaier[a] and Pavel A. Levkin*[ab]

Received 6th September 2016
Accepted 10th October 2016

DOI: 10.1039/c6ra22336b

www.rsc.org/advances

Superhydrophobic (SH) surfaces have various unique and important properties, including extreme water-repellency, self-cleaning, anti-icing and cell repellency. The range of applications and the interest in these surfaces have increased enormously during the last years. To obtain superhydrophobicity a surface requires both micro- and nano-scale roughness and a low surface energy coating. During the last 15 years many methods have been published to produce SH surfaces. Most of the methods described in the literature require multiple steps and harsh conditions. In addition, the comparability of the distinct studies is challenging, due to the fact that the produced surfaces were not characterized with sufficiently standardized parameters and methods. A comparative study with a wide space of parameters, characterizing both the method and the surface properties, could be helpful to find the right functionalization method for a certain application. The goal of this study was to compare the most facile methods for the fabrication of superhydrophobic surfaces. We selected eight coating methods and characterized produced surfaces in respect of water contact angles (WCAs) (static, advancing, receding), sliding angle, mechanical stability, stability in water/buffer/solvent, transparency and micro/nano surface topography.

Introduction

The interest in superhydrophobic (SH) surfaces and the efforts in producing surfaces with anti-wetting properties have been significantly increased during the last few years.[1–5] Starting off from mimicking natural surfaces with special properties like the self-cleaning lotus leaf,[6,7] research has brought up many applications of SH surfaces,[8,9] *e.g.* self-cleaning,[10] anti-icing,[11] anti-fogging[12] or anti-fouling coatings.[13] Another wide range of applications such as miniaturized separation and diagnostics or microarrays use functional patterns[8] that combine wettable and superhydrophobic or oil-repellant properties to create patterns or arrays of microdroplets of water[14] or other solvents.[15] SH surface modifications hold promise in smart microfluidic channels[16] and oil–water separation membranes.[17] However, simple methods that do not require either harsh conditions or multistep procedures are needed to facilitate the progress in this field.

Surfaces can be claimed as superhydrophobic when they show a water contact angle (WCA) of more than 150° and a low sliding angle or contact angle hysteresis (usually <10°).[18] There are two main models to describe the behavior of a water droplet on a rough surface. In the Wenzel state the water penetrates the cavities of a rough surface, which leads to an increased surface contact area and higher contact angles.[19] According to the Cassie–Baxter model, the water droplet rests on gas filled grooves of the rough surface, which often leads to superhydrophobicity with very low contact angle hysteresis and sliding angles.[20] An irreversible transition from the Cassie–Baxter state to the Wenzel state can often be observed, leading to an increase of CA hysteresis and loss of superhydrophobicity.[21–23]

It is generally accepted that surfaces need to fulfill two requirements to become superhydrophobic: a micro-/nano-rough structure[24] and low surface energy.[25] There are different approaches in generating surfaces with these properties. Some methods introduce surface roughness *via* phase separation,[26] electrospinning,[27] polymerization[28] or dip-coating.[29,30] Other strategies modify existing material by chemical[31,32] or plasma[33] etching to generate roughness. Often produced rough surfaces need to be modified with low surface energy functionalities, for example using self-assembling monolayers (SAMs)[29,30] or *via* click-chemistry.[34,35]

Despite the significant progress in the development of new methods for making superhydrophobic coatings, most of the existing approaches still require harsh conditions, many fabrication steps or special equipment.[27,29,32,36–39] For example, a typical layer-by-layer approach often needs 50–100 layers to generate the required surface properties[40] or has to be treated with temperatures >500 °C.[41] Nanotextured silica surfaces promise interesting combinations of properties like superhydrophobicity and

[a]*Institute of Toxicology and Genetics, Karlsruhe Institute of Technology (KIT), 76344 Eggenstein-Leopoldshafen, Germany. E-mail: levkin@kit.edu*

[b]*Institute of Organic Chemistry, Karlsruhe Institute of Technology (KIT), 76131 Karlsruhe, Germany*

† Electronic supplementary information (ESI) available. See DOI: 10.1039/c6ra22336b

transparency, but to produce them several steps are necessary, including baking at 500 °C, oxygen plasma etching and interference lithography.[38] Another important problem of superhydrophobic coatings is their low mechanical and chemical stability as well as the stability of the SH Cassie–Baxter state upon immersion in liquid.

Nevertheless, there are methods to produce SH surfaces in a simple and fast way. Here we give a few examples of the most facile methods. This list is however not comprehensive and there might be other simple approaches reported. Oliveira *et al.* provided a one-step method to create rough polystyrene *via* phase-separation on polystyrene Petri dishes.[26] Zhang *et al.* introduced a nanoporous poly(divinylbenzene) (PDVB) chalk for coating paper, polydimethylsiloxane (PDMS) and skin.[42] Another SH coating for paper made of hydrophobic silica nanoparticles was first produced by Ogihara *et al.* by a spray depositions technique[43] and later by Tang *et al. via* dip-coating.[44] Transparent coatings for glass slides *via* dip-coating and SAM were shown by Shang *et al.*[30] Different polymer coatings on glass were tested like poly(butyl methacrylate-*co*-ethylene dimethacrylate) (BMA-EDMA)[28] and fluorinated poly(2-hydroxyethyl methacrylate-*co*-ethylene dimethacrylate) (HEMA-EDMA) modified *via* the thiol-yne reaction.[34] The use of silica/polymer composites[45] and nano calcium carbonate/polymer composites[46] on glass substrate *via* brush coating was investigated by Tang *et al.*

The simplest method that could even be performed in the home kitchen is probably the deposition of candle soot that was described by Callies *et al.*[47] As there are already commercially available SH coatings, one of them was tested in this project.

It is often challenging to compare different methods, as the surface properties are usually characterized by only few methods, sometimes using only WCA measurements. Mechanical stability, resistance to solvents and buffers as well as stability of the Cassie–Baxter state and transparency are crucial for different applications but often not reported. In this study we used a wide range of parameters to characterize SH surfaces. As methods for the fabrication of SH coatings we selected the quickest and simplest methods that do not require specialized equipment and harsh conditions, thereby being most interesting for a wider range of possible applications. The methods are based on commercial starting reagents and the required equipment and glassware are usually available in any chemistry lab. Thus, all selected methods can be adopted and applied by almost any laboratory within a few days.

Experimental

Materials

Nexterion® Glass B slides were used as glass substrate and were obtained from Schott AG (Germany). 94 × 16 polystyrene Petri dish from Greiner Bio-One International GmbH (Austria) were used as polystyrene substrate. Printing paper Evolution White (Steinbeis Papier GmbH, Germany) was used as paper substrate. A deep UV collimated light source OAI Model 30 (San Jose, USA) with 500 W Hg-xenon lamp from USHIO (Japan) was used with UV power meter (OAI 360) with 260 nm probe head. Adhesive tape from Tesa (Germany) was used for the tape test.

Solvents

All solvents were used as received without further purification: deionized water (18.3 MΩcm), PBS buffer (DPBS 1×, Gibco, Thermo Fisher Scientific Inc., USA), ethanol (Absolut, Merck, Germany), toluene (reagent grade, Merck), tetrahydrofuran (HPLC grade, Sigma Aldrich, Germany), hexane (Suprasolv, Merck), ethyl acetate (Chromasolv, Sigma Aldrich), 1-decanol (Merck), cyclohexanol (Sigma Aldrich), dichloromethane (Emsure, Merck), acetone (Carl Roth, Germany), methanol (LiChrosolv, Merck).

Chemicals

The monomers for photopolymerization were purified by passing them through a short column packed with inhibitor remover (Sigma Aldrich). All other chemicals were used as received without further purification. The commercial sources of the chemicals are available as ESI.†

Coating procedures

The detailed coating procedures are available as ESI.†

Characterization

Water contact angle measurements. To determine the wetting properties of surfaces static (θ_s), advancing (θ_{adv}) and receding (θ_{rec}) water contact angles (WCAs) were measured. For θ_s 4 μL of deionized water were set onto the surface and the WCA was measured. The contact angle hysteresis $\Delta\theta$ was calculated as $\theta_{adv} - \theta_{rec}$. To measure θ_{adv} and θ_{rec} approximately 2 μL of water were added to/removed from the sessile droplet with a syringe pump (Microliter flow modular pump component, Harvard Apparatus, In. US.). The sliding angle (θ_{sl}) was measured with 4 μL of water set on the surface on a platform that could be tilted in a controlled way. All images of the droplets were taken with a UK 1115 digital camera from EHD imaging (Germany). ImageJ software with a DropSnake plugin was used to determine the contact angles. All WCA measurements were repeated at least three times. The results show the average value ± standard deviation.

Scanning electron microscopy. Scanning electron microscopy was performed with a LEO 1530 Gemini scanning electron microscope (Zeiss, Germany) at the Institute of Nanotechnology (INT), KIT. Before SEM measurements the samples were sputtered with a 30 nm gold layer using a Cressington 108 auto sputter coater (INT, KIT).

Tape test. To compare the mechanical stability of the SH coatings a simple tape test was carried out. A stripe of adhesive tape (Tesa, Germany) was stuck to the surface and pulled off. After that θ_s was measured again and the procedure was repeated several times.

Stability of the Cassie–Baxter state in water or buffer. For measuring the stability of the Cassie–Baxter state the samples were immersed in water/PBS buffer for a certain time. The

sample were taken out, the excess of water/buffer was removed by shaking the samples, and both θ_s and θ_{sl} were immediately measured.

Stability in solvents. The samples were immersed in acetone or ethanol, respectively for 1 h. After drying the samples, θ_s and θ_{sl} were measured.

UV/Vis. The UV/Vis transmittance was measured using a deuterium, halogen UV-VIS-NIR lightsource (DH-2000-BAL) and a high resolution spectrometer (HR2000+) from Ocean Optics Inc. (USA).

Results and discussion

Several methods were selected and compared in their SH properties and their mechanical stability as well as resistance against aqueous solutions and organic solvents. Transparency of the coatings was also characterized. A tape test was used to compare the mechanical stability. An adhesive tape was applied to the surface, pulled off and θ_s was measured again. Thin coating layers or mechanically unstable coatings are damaged by this test easily. In many studies a transition of the Cassie–Baxter state to the Wenzel state could be observed after a certain time.[21,26,40,48] To analyze the Cassie–Baxter stability, samples were immersed in water for different time periods. The samples were then taken out of water, the excess of water was removed by shaking the samples, and both θ_s and θ_{sl} were immediately measured. For many biological applications it is crucial that the surface properties do not deteriorate in the presence of buffer solutions. We used the most common buffer, phosphate-buffered saline (PBS), to immerse the samples and measure both θ_s and θ_{sl} after different periods of time. In many cases washing the surface with organic solvents is required for cleaning or as a part of the application. To test the stability of the surfaces against organic solvents the samples were immersed in acetone or ethanol for 1 h each and both θ_s and θ_{sl} were measured after drying the sample. Another important characteristic is the transparency of the coating.[49] This property was determined *via* measuring UV/Vis-transmittance through the coatings. To characterize the morphology of the surfaces, scanning electron microscope (SEM) images were taken.

Rough polystyrene

The SH polystyrene surface was produced as described by Oliveira *et al.*[26] Briefly, ethanol was added to a stock solution of polystyrene in tetrahydrofuran. A few drops of this solution were placed on the smooth polystyrene surface. After 5 s the substrate was immersed in ethanol, which led to a phase separation and the formation of the rough surface. This surface showed θ_s, θ_{adv} and θ_{rec} of 152°, 165° and 149°, respectively. The formation of rough polystyrene on the substrate did not occur homogeneous. This led to different wettabilities on the surface, as it can be seen in Fig. 1A. Particles with 1–10 μm size could be identified in the SEM images, forming pores smaller than 1 μm (Fig. 1C). This surface coating appears white and opaque, which is confirmed by the UV/Vis measurements (Fig. 1B).

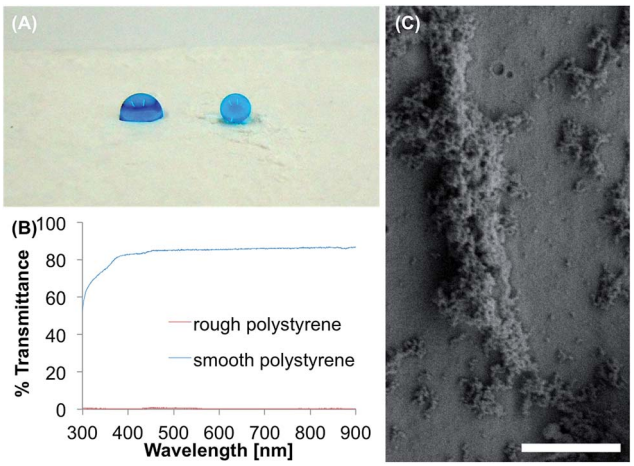

Fig. 1 Rough polystyrene. (A) Water droplets on a rough polystyrene surface. The randomly formed structure shows inhomogeneous wettability properties. The droplet on the left is pinned to the surface, while the droplet to the right can easily roll off. The water was colored with a food dye. (B) Light transmittance through smooth and rough polystyrene. While the smooth polystyrene shows a good transmittance of about 80% in the visible area, the roughness leads to an opaque surface (~0% transmittance). (C) SEM image of the rough polystyrene surface. The scale bar represents 10 μm. The surface shows both nano- and microrough structures.

The mechanical stability was investigated with a tape test. After five times of applying and pulling off the adhesive tape the θ_s decreased from 152° to 77°, which is close to the untreated, smooth polystyrene with θ_s of 73°. This indicates a loss of surface micro/nano roughness during this test. Two days after immersion in water the θ_s of the surface decreased only slightly from 152° to 141°. However, θ_{sl} increased from 10.3° to 23.3° after 48 h in water, indicating a transition from Cassie–Baxter state to Wenzel state. Incubation of the surface in PBS-buffer accelerated the loss of superhydrophobicity and θ_s of 110° was measured after 48 h. θ_{sl} could not be measured as the water droplet was pinned to the surface after immersion in buffer for 1 hour, indicating complete transformation to the Wenzel state. Immersion in acetone dissolved the polystyrene substrate, while immersion in ethanol for 1 hour did not decrease θ_s (153°) and only slightly increased θ_{sl} to 15.5°.

PDVB chalk

The divinylbenzene was polymerized in ethyl acetate with azobisisobutyronitril (AIBN) as initiator as described by Zhang *et al.*[42] to form poly(divinylbenzene) (PDVB). After 4 h of stirring at room temperature and 24 h of stirring at 80 °C the solvent was evaporated and the white solid was grinded to a fine powder. The substrate was a usual printing paper and was coated simply by scattering the polymer chalk onto the surface (Fig. 2A). θ_s, θ_{adv} and θ_{rec} proved the superhydrophobicity of the coating with values of 151°, 160° and 149° and θ_{sl} of 7.4°. The white particles surrounded a droplet of water on the surface immediately and the droplet rolled off the surface, similar to liquid marbles formed with SH powders.[50] In the SEM image, particles with

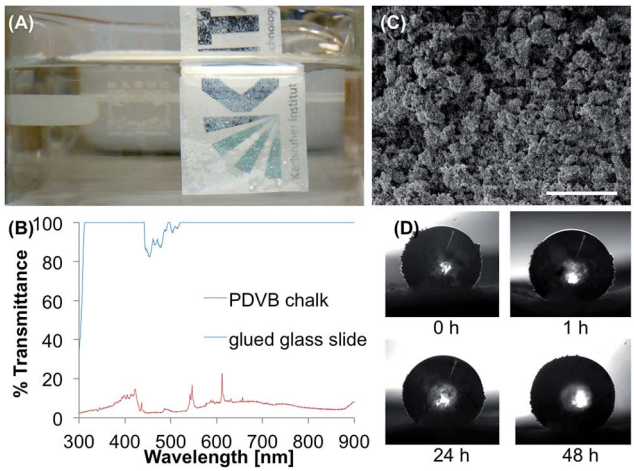

Fig. 2 PDVB chalk coated paper and glass. (A) Paper coated with PDVB chalk immersed in water. The SH coating protects the paper from wetting. (B) Transmittance of PDVB chalk glued on a glass slide (red). For comparison a glass slide was coated with glue (blue). The high transmittance of glued glass, nearly 100% from 310–900 nm, is reduced by the polymer chalk to a maximum value of 22% transmittance at 610 nm and less than 15% over the remaining range. (C) The SEM image of the PDVB chalk on paper (scale bar, 100 μm) shows particles of the PDVB in the microscale. (D) Water droplets on the PDVB chalk surface after repetitive immersion in water. Every immersion leads to a loss of particles that coat the droplet and make it roll off.

a size of 10–20 μm could be examined (Fig. 2C). The transparency could not be investigated on the paper substrate, so the PDVB chalk was glued onto a glass slide (Fig. 2B). For comparison another glass slide with glue was measured. The results show a maximum transmittance of 22% at 610 nm caused by the large size of the chalk particles.

In the tape test the coated paper lost its superhydrophobicity after five times of taping. θ_s decreased from 151° to 86°, which is close to θ_s of untreated printing paper (83°). In the stability tests in water and buffer θ_s decreased after 48 h to 135° and 131°, respectively. θ_{sl} decreased slightly for the coated paper in water to 4.9°. The water droplets on two-thirds of the samples did not roll off after 48 h of incubation in buffer, only one maintained a low θ_{sl} of 4.3°. Every immersion led to loss of particles, as Fig. 2D and Video S1† show. It is assumed that after the first immersion in water the biggest particles float away and the smaller particles lead to a decreased θ_{sl}. The images taken during the WCA measurements show the changing particle size and quantity. When the smaller particles are also washed away, the paper begins to soak water and loses its hydrophobicity. After immersion in acetone for 1 h θ_s decreased to 127° and the water droplet was pinned to the surface. In ethanol the structure of the surface was more stable (θ_s 149° after 1 h), however, the hydrophobic state changed from Cassie–Baxter to Wenzel model, as indicated by a pinned water droplet.

Spray-deposited silica nanoparticles

The hydrophobic silica nanoparticles were produced according to Ogihara *et al.*[43] SiO_2 nanoparticles with 10–20 nm particle size were stirred in toluene with dodecyltrichlorosilane under reflux for 3 h. After cooling, filtration and drying the particles were grounded to a fine powder that could be suspended in ethanol. With a glass vaporizer the suspension was sprayed onto paper (Fig. 3A). After drying the surface showed θ_s, θ_{adv} and θ_{rec} of 152°, 160° and 148°. θ_{sl} of 5.8° was measured. In Fig. 3C and D the SEM images show the nanoparticles covering the cellulose fibers. The particle size is mainly below 1 μm, but the particles also seem to form bigger agglomerates. The transmittance was investigated by gluing the silica nanoparticles on a glass slide the same way it was done for PDVB chalk. The results show that the coating is non-transparent (Fig. 3B) with a maximum transmittance of 19% at 612 nm.

Taping the surface five times led to a decrease of θ_s to 108°, which is still more hydrophobic than untreated printing paper (83°). Immersion of the coated paper in water for 48 h led to a θ_s of 58° and pinned water droplets. This loss of the superhydrophobicity was also observed after immersion in buffer. θ_s decreased to 47° after two days in buffer. Immersion of the surface in the buffer for only 1 h led to pinned water droplets. Immersion of the coated paper in organic solvents did not decrease θ_s significantly (acetone 151°, ethanol 152°) and only led to a small increase regarding θ_{sl} (acetone 20.6°, ethanol 17.5°).

Dip-coating and SAM

This modification of glass substrates consists of two steps. In the first step a silica nanoparticle colloidal solution was prepared from tetraethylorthosilicate in ethanol with ammonia as a catalyst according to Shang *et al.*[30] The cleaned glass substrate was dip-coated in this solution, dried for 5 min at ambient conditions

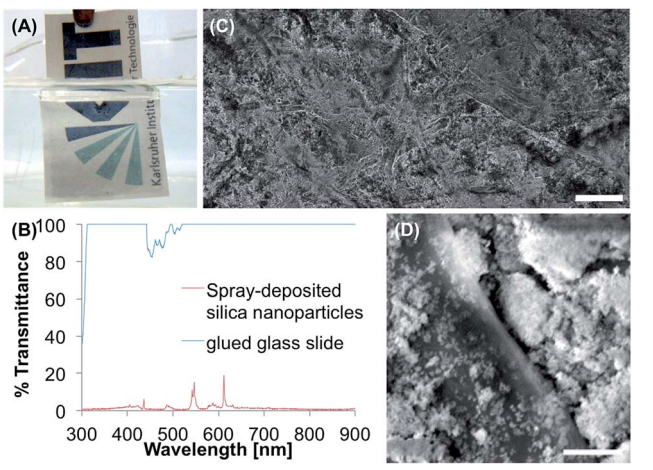

Fig. 3 Paper coated with silica nanoparticles. (A) Paper substrate treated with hydrophobic nanoparticles. The particles were sprayed as an ethanol suspension. (B) Transmittance through a layer of silica nanoparticles (red) glued to a glass slide. A glued glass slide without the nanoparticles for comparison (blue). Maximum transmittance values of the coating is 15% (546 nm) and 19% (612 nm). (C and D) SEM images of the nanoparticles on paper. The scale bars represent 100 μm (C) and 2 μm (D), respectively. In (D) a cellulose fiber, covered by nanoparticles, is visible.

and for 1.5 h at 80 °C. In the second step, the silica surface was coated with a self-assembling monolayer (SAMs) of tridecafluoro-1,1,2,2-tetrahydrooctyldimethylchlorosilane (TFCS) by immersing the surface in hexane solution of TFCS for at least 6 h. The modified glass (Fig. 4A) showed θ_s, θ_{adv} and θ_{rec} of 138°, 156° and 127°. According to the literature these properties, including θ_{sl} of 55.5°, do not suffice to call the surface superhydrophobic.[18] Still the surface is hydrophobic and shows nearly 100% transmittance at 300–900 nm (Fig. 4B). The SEM images show an unequal distribution of particles with sizes from 1–100 μm (Fig. 4C and D). The particles don't cover the whole surface, which is probably the reason for the low WCAs.

During the tape test θ_s decreased constantly to 91° after five times of applying the tape. For comparison, the unmodified, cleaned glass slide showed a θ_s of 41°. The coated glass lost its hydrophobicity during immersion in water slowly, but continually. After 48 h in water, θ_s dropped to 128° and the water droplets were pinned to the surface. In buffer, θ_s decreased to 119° after 48 h and after 24 h the water droplets didn't roll off the surface anymore. After immersion in ethanol for 1 h, θ_s decreased to 128°, in acetone it decreased even more to 117°. In both cases the water droplets did not roll off the surface again.

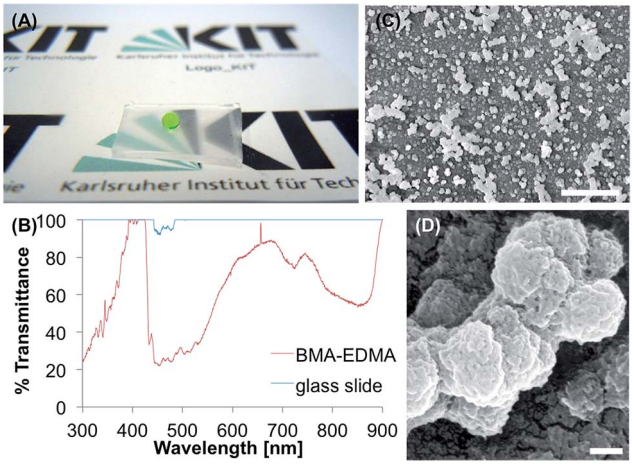

Fig. 5 Macroporous BMA-EDMA polymethacrylate coating. (A) BMA-EDMA on a glass substrate with a colored water droplet. (B) Transmittance of the BMA-EDMA coating on glass, compared to an untreated glass substrate. The polymer shows increasing transmittance from 300–400 nm (24–100%) and a sudden drop to 22% at 450 nm. In the range from 450–900 nm the polymer reduces the transmittance of the glass slide to values between 23–98%. (C and D) SEM images of the nano-micro rough BMA-EDMA surface (C: scale bar 10 μm, D: scale bar 200 nm).

Porous BMA-EDMA polymer coating

The porous poly(butyl methacrylate-*co*-ethylene dimethacrylate) (BMA-EDMA) coating was produced on a glass substrate according to Levkin *et al.*[28] *via* photopolymerization corresponding methacrylate monomers between two glass slides. The pore size was controlled by the amount of 1-decanol and cyclohexanol in the polymerization mixture. The BMA-EDMA surface (Fig. 5A) reached θ_s, θ_{adv}, and θ_{rec}, values of 160°, 166° and 151° and θ_{sl} of 5.7°. On the surface particles with sizes in the range of 100–400 nm formed agglomerates up to 10 μm (Fig. 5C and D). The polymer is transparent at 390–420 nm and at 900 nm (100% transmittance), but non-transparent in the range of 430–550 nm (22–45% transmittance) (Fig. 5B).

In the tape test, θ_s decreased to 101° after five times of applying the tape. The immersion in water for 1 h led to a decrease of θ_s to 143° and an increase of θ_{sl} from 5.7° to 46.0°, indicating transition to the Wenzel state, after 24 h the surface became hydrophilic ($\theta_s = 0°$). In the buffer, the surface showed similar behavior with θ_s of 144° and θ_{sl} of 42.0° after 1 h of immersion and θ_s of 0° after 24 h. Organic solvents led to a small decrease of the superhydrophobicity with θ_s of 158° and θ_{sl} of 8.6° for acetone and θ_s of 157° and θ_{sl} of 6.8° for ethanol.

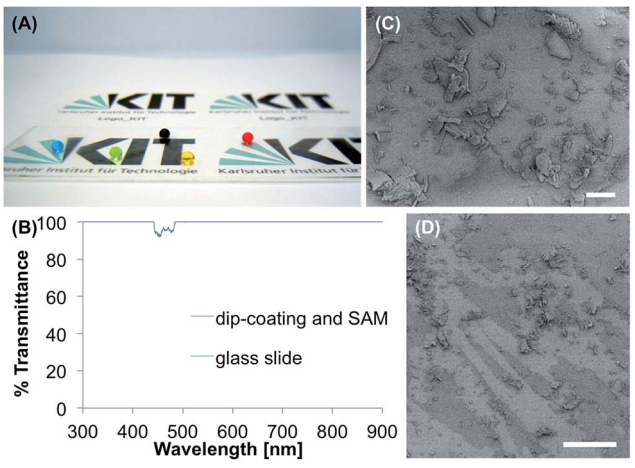

Fig. 4 Dip-coating using colloidal silica nanoparticles followed by silanization. (A) Food-dye colored water droplets on a glass slide coated *via* dip-coating in silica-based sols and SAMs (self assembling monolayers). (B) Transmittance of the dip-coating and SAM. For comparison, an untreated glass slide was also measured. The coating does not influence the transmittance of the glass substrate of nearly 100% at 300–900 nm. (C and D) SEM images of the coated surfaces. Scale bars 20 μm (C) and 100 μm (D), respectively. Microscale particles can be observed.

Modified porous HEMA-EDMA polymer

The modified poly(2-hydroxyethyl methacrylate-*co*-ethylene dimethacrylate) (HEMA-EDMA) coating was produced according to the following steps, reported by Feng *et al.*[34] First, a thin porous polymer layer (12.5 μm) of HEMA-EDMA was prepared on a glass slide through photopolymerization, as firstly introduced by Geyer *et al.*[51] The surface was esterified with 4-pentynoic acid. The terminal alkyne groups could be modified easily by UV-initiated thiol-yne click reaction. For a SH surface the used thiol was 1*H*,1*H*,2*H*,2*H*-perfluorodecanethiol and led to θ_s, θ_{adv} and θ_{rec} of 152°, 158° and 143°, respectively. The average θ_{sl} was 6.3°. A coated glass substrate is shown in Fig. 6A. The SEM images (Fig. 6C and D) show a homogenous distribution of the porous polymer on the substrate. The pore size is in the range of several hundred nanometers. The polymer coating is not completely transparent (Fig. 6B). Below 530 nm the transmittance is less

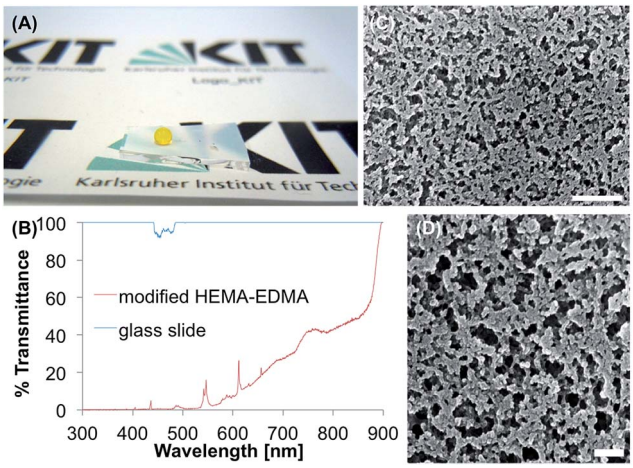

Fig. 6 Nanoporous HEMA-EDMA polymethacrylate coating. (A) A thin layer of modified HEMA-EDMA on glass. The water droplet was colored with a food dye. (B) Transmittance of the polymer film compared to an untreated glass slide. The polymer is opaque (<1% transmittance) in the range from 300–530 nm. From 530–900 nm the transmittance increases constantly until it reaches 100% at 900 nm. (C and D) SEM images of the HEMA-EDMA sample, the scale bars represent 1 μm (C) and 300 nm (D), respectively.

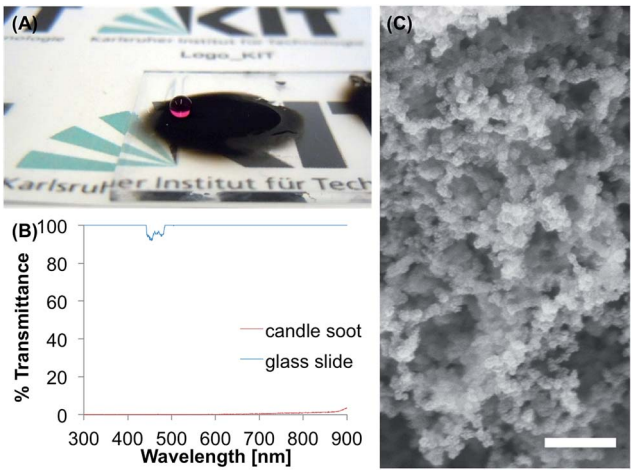

Fig. 7 Candle soot coating. (A) Candle soot deposited on a glass slide simply by holding a glass slide over a burning candle. The darkened area shows superhydrophobic behavior. (B) The black candle soot is completely non-transparent (red), as seen from the UV/Vis measurements. Over the range from 300–900 nm the transmittance stays below 3%. (C) SEM image of the wax nanoparticles in the candle soot. The scale bar represents 300 nm.

than 1%. Between 700–800 nm the transmittance reaches a local maximum of 43%. From 850–900 nm the transmittance increases to 100%.

It was already recognized by Geyer *et al.* that applying adhesive tape to the surface leads to a higher roughness and more superhydrophobic properties of the coating. This could be confirmed with the tape test in this study. After five times of applying the tape, θ_s indeed increased from 152° to 157°. To intensify the conditions of the test, the tape was applied 20 times. After 10 times θ_s continued to increase up to 160°, only after 20 times θ_s decreased to 135°. The immersion of the surface in water for 48 h led to a θ_s of 146° and θ_{sl} of 26.2°. After 48 h in buffer the surface showed a θ_s of 139° and θ_{sl} of 56.4°. Ethanol did not influence θ_s of the polymer surface, while acetone even increased it slightly to 155°. θ_{sl} increased in both cases to 14.3° and 12.3°, respectively.

Candle soot

Candle soot, that was simply deposited on the substrate by holding a glass slide over a candle, led to a superhydrophobic surface (Fig. 7A) with θ_s, θ_{adv} and θ_{rec} of 152°, 156° and 140° and θ_{sl} of 11.3°. The candle soot was already used as a template for a stable SH surface made of silica shells by Deng *et al.*[52] The particles that could be observed in the SEM (Fig. 7C) show a spherical shape with the size of tens of nanometers. The candle soot is non-transparent from 300–900 nm with less than 3% transmittance within the complete range (Fig. 7B).

The tape test led to a complete loss of the superhydrophobicity, after applying the tape five times, with a θ_s of 44°. Immersion in water for 48 h also decreased θ_s to 43° and water droplets were pinned to the surface even after 1 h of the immersion time. In buffer, the surface became completely hydrophilic with θ_s of 0° after 1 h immersion. Ethanol and acetone led to θ_s of 114° and 48°, respectively, and to pinned water droplets.

Commercial coating

The commercial coating consists of two layers (bottom and top layer), that are sprayed onto the surface. For the tests ready-made sample tiles on a ceramic substrate were used (Fig. 8A).

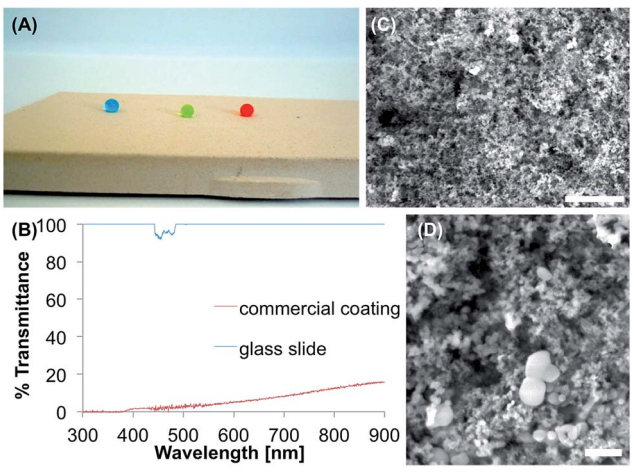

Fig. 8 Commercial superhydrophobic coating on a ceramic tile and glass slide. (A) Colored water droplets on a ceramic tile coated with the commercial coating. (B) Light transmittance of the commercial coating formed on a glass slide. The coating leads to a non-transparent surface with less than 2% transmittance in the range from 300–400 nm and a slightly increasing transmittance with a maximum value of 15% (900 nm) in the range from 400–900 nm. (C and D) SEM images of the coating on a glass substrate. The scale bar represent 1 μm (C) and 200 nm (D), respectively. The coating shows a nanorough surface.

The surface showed θ_s, θ_{adv} and θ_{rec} of 155°, 166° and 152°, and θ_{sl} of 14.8°. For the SEM images and the UV/Vis measurements the coating was prepared on a glass substrate. The SEM images (Fig. 8C and D) show particles in the range of 10–100 nm that cover the substrate and form a nanorough surface with pores up to 200 nm. The coating is opaque (0% transmittance) in the range from 300–380 nm (Fig. 8B), while increasing linearly to a maximum value of 16% at 900 nm.

After applying adhesive tape for five times to the surface, θ_s decreased to 122°. Immersion in water for two days led to a θ_s of 143° and an increased θ_{sl} of 37.6°. In the PBS buffer, θ_s of 142° and θ_{sl} of 44.7° were reached after 48 h. Ethanol led to a slightly decreased θ_s of 151° and θ_{sl} of 21.3°, while acetone led to a θ_s of 153° and θ_{sl} of 29.8°.

Comparison and summary

Eight methods were used to produce superhydrophobic coatings. The surfaces were characterized by WCAs, mechanical stability, stability of the Cassie–Baxter state upon immersing the surfaces in water or buffer and the resistance to organic solvents as well as transparency and surface topography at the micro-nano scale. The results obtained from the different measurements indicate advantages and disadvantages of the compared coatings that can be useful for their applications. The results are summarized in Table 1.

Water contact angles

As the main indicator of superhydrophobicity the static, advancing and receding WCAs play an important role (Fig. 9). The θ_s of 150°, which is commonly used to declare a surface as superhydrophobic was reached by all tested methods, except the dip-coating method. The SEM images of the dip-coated glass slide also indicated incomplete coverage of the substrate, which is probably the reason for the low θ_s. The highest θ_s was reached by the BMA-EDMA coating.

The small difference between θ_{adv} and θ_{rec}, contact angle hysteresis, is also an important indicator for superhydrophobicity. As alternative, θ_{sl} below 10° can be used. θ_{adv} and θ_{rec} and θ_{sl} of the surfaces produced in this study are shown in Fig. 9. The BMA-EDMA surface shows the lowest θ_{sl} of 5.7°. Also the spray-deposited silica nanoparticles, the modified HEMA-EDMA and the PDVB chalk reached θ_{sl} below 10°. The candle soot, the rough polystyrene and the commercial coating, possessed values of θ_{sl} between 10° and 15°. Nevertheless, the receding contact angles measured on most of the surfaces were below 150°.

Tape test

The results of the tape test, reflecting the resistance of the coatings to mechanical damage, are shown comparatively in Fig. 10. Most of the coatings lost their superhydrophobicity already after the first application of the tape as indicated by the decrease of θ_s below 150° and below 130° after two tape applications.

Table 1 Results of the characterization of the different superhydrophobic coatings. The investigated properties include transparency (UV/Vis), WCAs (θ_s, θ_{adv} and θ_{rec}), sliding angle (θ_{sl}), mechanical stability (tape test) and stability in water, PBS-buffer and organic solvents. * indicates that water droplet did not roll off the surface

Surface	Rough polystyrene	Nanoporous PDVB chalk	Spray-deposited silica nanoparticles	Dip-coating and SAM	BMA-EDMA	Modified HEMA-EDMA	Candle soot	Commercial coating
Transparency	<1%	max. 22% (610 nm)	max. 19% (612 nm)	100%	22–100%	<1% (300–500 nm), max. 100% (900 nm)	<2%	<1% (300–400 nm), max. 16% (900 nm)
θ_s, θ_{adv}, θ_{rec} [°]	152.1 ± 1.8, 164.7 ± 0.5, 148.6 ± 0.5	151.3 ± 1.4, 159.9 ± 0.5, 148.5 ± 0.5	151.7 ± 1.1, 159.6 ± 0.3, 147.6 ± 1.7	137.7 ± 4.5, 155.7 ± 1.0, 126.9 ± 2.6	160.2 ± 0.6, 165.8 ± 0.7, 150.7 ± 3.2	152.0 ± 3.6, 158.2 ± 0.6, 142.9 ± 2.4	151.6 ± 1.7, 155.8 ± 0.3, 140.3 ± 2.4	154.7 ± 1.4, 166.5 ± 0.8, 152.4 ± 1.2
Sliding angle [°]	13.9 ± 3.8	7.4 ± 1.5	5.8 ± 2.4	55.5 ± 5.2	5.7 ± 1.1	6.3 ± 1.6	11.3 ± 2.1	14.8 ± 3.4
Mechanical stability (θ_s after 5× tape test) [°]	77.1 ± 1.8	86.4 ± 4.0	108.4 ± 1.8	90.83 ± 2.8	101.4 ± 2.0	157.3 ± 0.9	43.9 ± 9.4	122.1 ± 1.0
Stability in water (immersion for 48 h) (θ_s [°], sliding angle [°])	140.8 ± 2.1, 23.3 ± 3.2	134.7 ± 4.1, 4.9 ± 1.1	58.1 ± 10.1, *	128.2 ± 1.1, *	0°, *	145.6 ± 3.2, 26.2 ± 3.7	42.8 ± 2.2, *	143.4 ± 1.3, 37.6 ± 1.8
Stability in buffer (immersion for 48 h) (θ_s [°], sliding angle [°])	110.4 ± 38.4, *	130.6 ± 4.5, *	47.2 ± 4.3, *	118.7 ± 1.3, *	0°, *	139.4 ± 7.2, 56.4 ± 0.1	0°, *	142.2 ± 2.2, 44.7 ± 6.0
Stability in acetone (immersion for 1 h) (θ_s [°], sliding angle [°])	Dissolved	127.1 ± 11.0, *	151.0 ± 0.6, 20.6 ± 6.2	117.4 ± 10.7, *	157.8 ± 0.2, 8.6 ± 1.8	154.6 ± 0.6, 12.3 ± 1.9	48.0 ± 2.6, *	152.7 ± 0.5, 29.8 ± 0.4
Stability in ethanol (immersion for 1 h) (θ_s [°], sliding angle [°])	Dissolved	148.9 ± 1.5, *	151.9 ± 0.7, 17.5 ± 2.8	128.1 ± 4.2, *	156.9 ± 0.5, 6.8 ± 1.3	152.3 ± 1.2, 14.3 ± 1.5	114.0 ± 20.4, *	150.8 ± 0.6, 21.3 ± 1.2
Reference for method	23	39	40	27	25	28 and 42	43	—

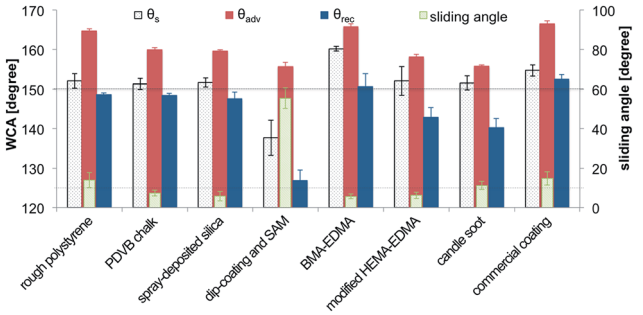

Fig. 9 Comparison of θ_s, θ_{adv} and θ_{rec} (left y-axis) and θ_{sl} (right y-axis) measured in this study. The results are sorted by the different surfaces (x-axis) and the error bars show the standard deviation. The upper dashed line indicates 150°, the lower dashed line indicates θ_{sl} of 10°.

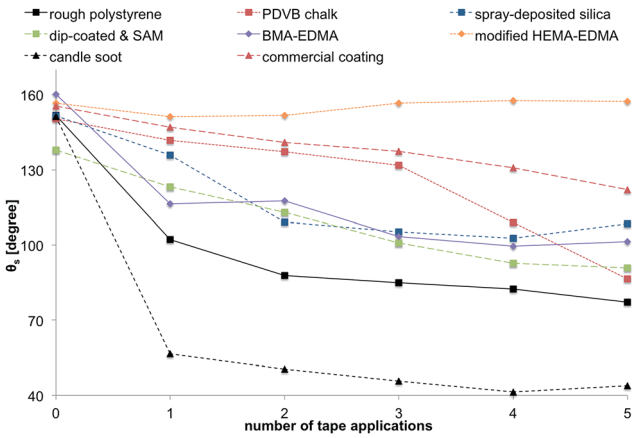

Fig. 10 Results of the tape test. The different surfaces were treated with adhesive tape for five times, whilst measuring θ_s.

One time application of adhesive tape to the surface the candle soot resulted in the complete loss of its superhydrophobic properties. The most stable coatings were the HEMA-EDMA, commercial one and the PDVB chalk. However, the latter two lost superhydrophobicity after 5 tape applications. Interestingly, not only the modified HEMA-EDMA did not lose its superhydrophobicity after taping, but θ_s even increased after applying the taping further. This effect is the result of the roughness of the HEMA-EDMA surface that originates from its porous structure and a relatively large thickness of this porous layer, as opposed to the two-dimensional roughness of other surfaces.[3,53,54]

Stability of the CB state

It is known that the Cassie–Baxter state is thermodynamically unstable and irreversible transition to the Wenzel state is possible, leading to the loss of superhydrophobicity. To compare the stability of the Cassie–Baxter state on the tested surfaces, we measured both θ_s and θ_{sl} on surfaces immersed into water or buffer for different time periods. Decrease of θ_s and large increase of θ_{sl} would indicate the transition to the Wenzel state and corresponding loss of superhydrophobicity. The results of the stability test in water are shown in Fig. 11. All surfaces showed a decrease of θ_s after immersion in water and

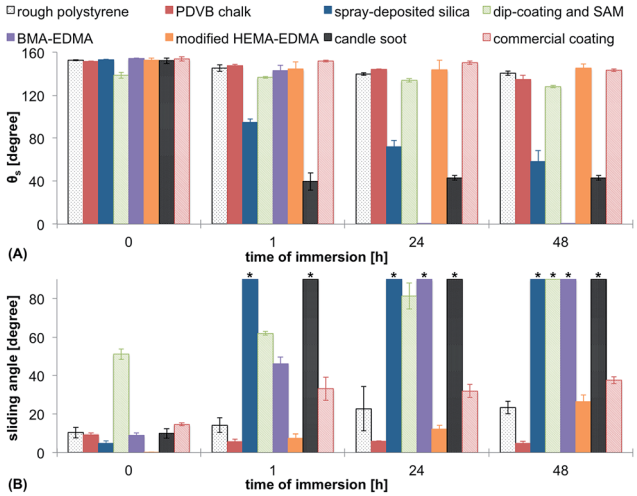

Fig. 11 Stability of the Cassie–Baxter state in water. θ_s (A) and θ_{sl} (B) of the surfaces were measured on surfaces incubated in water for different time periods. The measurements were performed immediately after taking the samples out water without drying to assess the Cassie–Baxter to Wenzel transition. All measurements were performed as triplicates and the error bars indicate the standard deviation. * indicates that water droplet did not roll off the surface.

an increase of θ_{sl}. The candle soot was washed off the glass substrate immediately after immersion in water and led to a hydrophilic surface. The BMA-EDMA surface became completely hydrophilic after one day of immersion. The spray-deposited silica nanoparticles also showed a severe loss of hydrophobicity during the test. The most stable coatings in this test were the modified HEMA-EDMA, the commercial coating and the rough polystyrene. θ_{sl} of the PDVB chalk surface stayed below 10° alone.

CB stability in buffer

The stability test in buffer showed the same trends as in the case of water, however, the decrease of θ_s and increase of θ_{sl} was more pronounced (Fig. 12). The only surfaces that did not show a pinned droplet in this test after 48 h of incubation were the modified HEMA-EDMA and the commercial coating.

Organic solvents

Resistance to solvents can be important in various applications of superhydrophobic coatings. Cleaning, recovery of the original properties or chemical functionalization often require incubation in organic solvents. Our last stability test involved incubation of the coatings either in acetone or ethanol for 1 h, followed by drying and measuring θ_s. The results are shown in Fig. 13. The rough polystyrene was completely dissolved in acetone, so there could not be any values obtained for this material. Acetone led to a significantly decreased θ_s for the PDVB chalk, dip-coating method and candle soot. For these surfaces also pinning of water droplets could be observed following the treatment with organic solvents. The immersion in ethanol led to similar results. The three mentioned surfaces became sticky towards water droplets and showed the lowest θ_s.

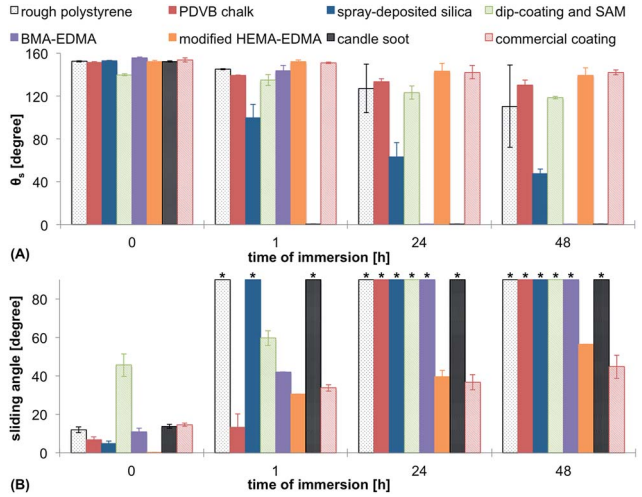

Fig. 12 Stability of the Cassie–Baxter state in buffer. θ_s (A) and θ_{sl} (B) of the surfaces were measured on surfaces incubated in PBS-buffer for different time periods. The measurements were performed immediately after taking the samples out buffer without drying to assess the Cassie–Baxter to Wenzel transition. All measurements were performed as triplicates and the error bars indicate the standard deviation. * indicates that water droplet did not roll off the surface.

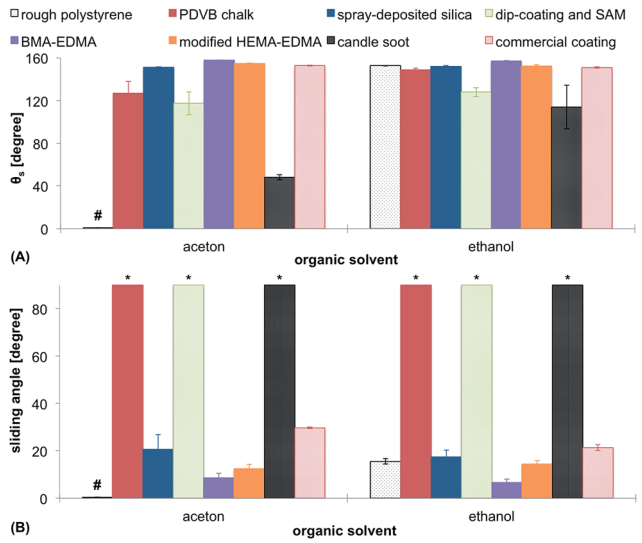

Fig. 13 Stability in organic solvents. The surfaces were immersed in acetone or ethanol for 1 h and θ_s (A) and θ_{sl} (B) were measured. * indicates that water droplet did not roll off the surface, # indicates that the sample dissolved in the solvent.

In comparison to acetone, ethanol did not influence the hydrophobicity of rough polystyrene. BMA-EDMA, modified HEMA-EDMA, spray-deposited silica nanoparticles and the commercial coating did not show significant changes in their superhydrophobic behavior.

Conclusions

Superhydrophobicity is a unique and important property that can be helpful in a variety of applications. Despite a lot of research and many reported fabrication methods, many of the existing methods require either harsh conditions or multiple steps including sophisticated equipment and, therefore, not easily transferrable to the field of applications. Nevertheless, a number of simple and rapid fabrication methods have been reported. In this study, we attempted to reproduce the simplest and most convenient methods and perform a comparative investigation of the properties of the produced superhydrophobic surfaces.

The main conclusion from this study is that there are indeed simple methods for the fabrication of superhydrophobic coatings that require 1 or 2 steps and do not need complex equipment or harsh conditions. All coatings in this study, except for one, showed superhydrophobic properties when freshly produced. However, none of these coatings possessed static contact angles above 160° or sliding angles below 5°. The mechanical stability of the produced coatings is very limited and none of the studied techniques provide long-term stability of the Cassie–Baxter state even upon incubation in water or PBS buffer. Irreversible transition to the Wenzel state with inevitable loss of superhydrophobicity was observed for all studied coatings, indicating a need for more research aiming at more stable and durable but at the same time simple approaches to superhydrophobic coatings. Several coatings were also either soluble or unstable in organic solvents.

The modified HEMA-EDMA, PDVB chalk and the commercial coating possessed the most robust superhydrophobic properties. The only surface resistant to multiple tape test applications was the modified HEMA-EDMA porous polymer, where the contact angle even increased after the initial tape treatment. This demonstrates the importance of porosity and thickness of the coating that endow them with better mechanical stability and resistance to erosion in comparison to thin or non-porous coatings.

These simple tests demonstrate the vulnerability of superhydrophobic surfaces and should help to plan correct experiments to design and evaluate novel simple but robust superhydrophobic coatings, which are crucial for the development of functional coatings for numerous applications.

Acknowledgements

We thank Konstantin Demir (Levkin group, KIT) for the production of the polymer surfaces and Ivana Pini (Levkin group, KIT) for the production of the commercial coating and the support with the SEM images. Further we thank the INT (KIT, Karlsruhe NanoMicro Facility) for giving access to the SEM instrument.

Notes and references

1 X. Feng and L. Jiang, *Adv. Mater.*, 2006, **18**, 3063–3078.
2 T. Sun, L. Feng, X. Gao and L. Jiang, *Acc. Chem. Res.*, 2005, **38**, 644–652.
3 T. Verho, C. Bower, P. Andrew, S. Franssila, O. Ikkala and R. H. A. Ras, *Adv. Mater.*, 2011, **23**, 673–678.

4 S. Subhash Latthe, *J. Surf. Eng. Mater. Adv. Technol.*, 2012, **2**, 76–94.
5 X.-M. Li, D. Reinhoudt and M. Crego-Calama, *Chem. Soc. Rev.*, 2007, **36**, 1350.
6 W. Barthlott and C. Neinhuis, *Planta*, 1997, **202**, 1–8.
7 Y. Y. Yan, N. Gao and W. Barthlott, *Adv. Colloid Interface Sci.*, 2011, **169**, 80–105.
8 E. Ueda and P. A. Levkin, *Adv. Mater.*, 2013, **25**, 1234–1247.
9 X. Yao, Y. Song and L. Jiang, *Adv. Mater.*, 2011, **23**, 719–734.
10 V. A. Ganesh, H. K. Raut, A. S. Nair and S. Ramakrishna, *J. Mater. Chem.*, 2011, **21**, 16304.
11 S. Farhadi, M. Farzaneh and S. A. Kulinich, *Appl. Surf. Sci.*, 2011, **257**, 6264–6269.
12 X. Gao, X. Yan, X. Yao, L. Xu, K. Zhang, J. Zhang, B. Yang and L. Jiang, *Adv. Mater.*, 2007, **19**, 2213–2217.
13 J. Kuang and P. B. Messersmith, *Langmuir*, 2012, **28**, 7258–7266.
14 E. Ueda, F. L. Geyer and P. A. Levkin, *Lab Chip*, 2012, 5218–5224.
15 W. Feng, L. Li, X. Du, A. Welle and P. A. Levkin, *Adv. Mater.*, 2016, **28**, 3202–3208.
16 L. Ionov, N. Houbenov, A. Sidorenko, M. Stamm and S. Minko, *Adv. Funct. Mater.*, 2006, **16**, 1153–1160.
17 L. Feng, Z. Zhang, Z. Mai, Y. Ma, B. Liu, L. Jiang and D. Zhu, *Angew. Chem., Int. Ed.*, 2004, **43**, 2012–2014.
18 D. Öner and T. J. McCarthy, *Langmuir*, 2000, **16**, 7777–7782.
19 R. N. Wenzel, *J. Ind. Eng. Chem.*, 1936, **28**, 988–994.
20 A. B. D. Cassie and S. Baxter, *Trans. Faraday Soc.*, 1944, **40**, 546.
21 E. Ueda and P. A. Levkin, *Adv. Healthcare Mater.*, 2013, **2**, 1425–1429.
22 J. Zhang and S. Seeger, *Angew. Chem., Int. Ed.*, 2011, **50**, 6652–6656.
23 T. Verho, J. T. Korhonen, L. Sainiemi, V. Jokinen, C. Bower, K. Franze and S. Franssila, *Proc. Natl. Acad. Sci. U. S. A.*, 2012, **109**, 10210–10213.
24 Z. Yoshimitsu, A. Nakajima, T. Watanabe and K. Hashimoto, *Langmuir*, 2002, **18**, 5818–5822.
25 R. Blossey and C. Scientifique, *Nat. Mater.*, 2003, 301–306.
26 S. M. Oliveira, W. Song, N. M. Alves and J. F. Mano, *Soft Matter*, 2011, **7**, 8932.
27 M. Ma, M. Gupta, Z. Li, L. Zhai, K. K. Gleason, R. E. Cohen, M. F. Rubner and G. C. Rutledge, *Adv. Mater.*, 2007, **19**, 255–259.
28 P. A. Levkin, F. Svec and J. M. J. Fréchet, *Adv. Funct. Mater.*, 2009, **19**, 1993–1998.
29 S. Nishimoto, A. Kubo, K. Nohara, X. Zhang, N. Taneichi, T. Okui, Z. Liu, K. Nakata, H. Sakai, T. Murakami, M. Abe, T. Komine and A. Fujishima, *Appl. Surf. Sci.*, 2009, **255**, 6221–6225.
30 H. M. Shang, Y. Wang, S. J. Limmer, T. P. Chou, K. Takahashi and G. Z. Cao, *Thin Solid Films*, 2005, **472**, 37–43.
31 D. Qi, N. Lu, H. Xu, B. Yang, C. Huang, M. Xu, L. Gao, Z. Wang and L. Chi, *Langmuir*, 2009, **25**, 7769–7772.
32 G. Piret, E. Galopin, Y. Coffinier, R. Boukherroub, D. Legrand and C. Slomianny, *Soft Matter*, 2011, **7**, 8642.
33 B. Balu, V. Breedveld and D. W. Hess, *Langmuir*, 2008, **24**, 4785–4790.
34 W. Feng, L. Li, E. Ueda, J. Li, S. Heißler, A. Welle, O. Trapp and P. A. Levkin, *Adv. Mater. Interfaces*, 2014, **1**, 1400269.
35 J. Li, L. Li, X. Du, W. Feng, A. Welle, O. Trapp, M. Grunze, M. Hirtz and P. A. Levkin, *Nano Lett.*, 2015, **15**, 675–681.
36 S. J. Pastine, D. Okawa, B. Kessler, M. Rolandi, M. Llorente, A. Zettl and J. M. J. Fréchet, *J. Am. Chem. Soc.*, 2008, **130**, 4238–4239.
37 D. Tian, Q. Chen, F. Q. Nie, J. Xu, Y. Song and L. Jiang, *Adv. Mater.*, 2009, **21**, 3744–3749.
38 K. C. Park, H. J. Choi, C. H. Chang, R. E. Cohen, G. H. McKinley and G. Barbastathis, *ACS Nano*, 2012, **6**, 3789–3799.
39 Y. Wu, H. Sugimura, Y. Inoue and O. Takai, *Chem. Vap. Deposition*, 2002, **8**, 47–50.
40 M. E. Buck, S. C. Schwartz and D. M. Lynn, *Chem. Mater.*, 2010, **22**, 6319–6327.
41 J. Bravo, L. Zhai, Z. Wu, R. E. Cohen and M. F. Rubner, *Langmuir*, 2007, **23**, 7293–7298.
42 Y.-L. Zhang, J.-N. Wang, Y. He, Y. He, B.-B. Xu, S. Wei and F.-S. Xiao, *Langmuir*, 2011, **27**, 12585–12590.
43 H. Ogihara, J. Xie, J. Okagaki and T. Saji, *Langmuir*, 2012, **28**, 4605–4608.
44 X. Tang, S. Nan, T. Wang, Y. Chen, F. Yu, G. Zhang and M. Pei, *RSC Adv.*, 2013, **3**, 15571–15575.
45 X. Tang, T. Wang, F. Yu, X. Zhang, Q. Zhu, L. Pang, G. Zhang and M. Pei, *RSC Adv.*, 2013, **3**, 25670–25673.
46 X. Tang, F. Yu, W. Guo, T. Wang, Q. Zhang, Q. Zhu, X. Zhang and M. Pei, *New J. Chem.*, 2014, **38**, 2245–2249.
47 M. Callies and D. Quéré, *Soft Matter*, 2005, **1**, 55.
48 A. Lafuma and D. Quéré, *Nat. Mater.*, 2003, **2**, 457–460.
49 E. Celia, T. Darmanin, E. Taffin de Givenchy, S. Amigoni and F. Guittard, *J. Colloid Interface Sci.*, 2013, **402**, 1–18.
50 P. Aussillous and D. Quéré, *Nature*, 2001, **411**, 924–927.
51 F. L. Geyer, E. Ueda, U. Liebel, N. Grau and P. A. Levkin, *Angew. Chem., Int. Ed.*, 2011, **50**, 8424–8427.
52 X. Deng, L. Mammen, H.-J. Butt and D. Vollmer, *Science*, 2012, **335**, 67–70.
53 P. Auad, E. Ueda and P. A. Levkin, *ACS Appl. Mater. Interfaces*, 2013, **5**, 8053–8057.
54 H. Jin, X. Tian, O. Ikkala and R. H. A. Ras, *ACS Appl. Mater. Interfaces*, 2013, **5**, 485–488.